ISSN: 2456-9348
Vol (02) _Issue (03) Impact Factor: 4.520

iJETRM
International Journal of Engineering Technology Research & Management

MODELING AND CONTROL OF HYBRID PV-WIND ENERGY GENERATION SYSTEM FOR EFFICIENCY IMPROVEMENT

Salama Abu-Zaid Abo-Alela
Electrical Engineering Department, El-Azhar University, Cairo, Egypt.
slama.abo@gmail.com

ABSTRACT
Renewable energy sources have attracted wide attention due to their advantages of being abundant in nature and nearly non-polluting. The most feasible and reliable Grid connected renewable energy systems are the hybrid wind-solar sources. This paper proposes a high performance power generation of hybrid solar photovoltaic (PV) with a large capacity doubly fed induction generator (DFIG) based wind energy system. The proposed scheme uses both the grid side converter (GSC) and rotor-side converter (RSC) of DFIG to inject PV power to the grid. This proposed scheme provides an elegant and economic integration of PV source and DFIG-based wind energy source. A Maximum Power Point Tracking (MPPT) extracted from the wind based rotor speed control is proposed in conjunction with pitch control to avoid overloading in case of high wind velocity over the rated value. The integrated GSC and RSC control is designed to implement the dc-link voltage control, active and reactive power, and grid voltage support control functions. The PV solar is connected directly to the dc-link. A nonlinear control is applied to extract Maximum Power from the PV under variable operating conditions. The proposed scheme does not hamper MPPT of PV and wind sources except during very rarely occurring environmental glitches, which the PV power control algorithm is suitably geared to handle using an artificial neural network (ANN). The developed model is validated through a comprehensive set of simulation studies in the Matlab/Simulink environments. A series of results are obtained in order to analysis the system performance under variable operating conditions.

Keywords:
Hybrid, PV, MPPT, DFIG, RSC, GSC, Matlab.

. INTRODUCTION

Due to the increasing concern about CO2 emissions, renewable energy systems and especially wind energy generation and photovoltaic (PV) generation systems have attracted great interests in recent years [1]. PV energy appears quite attractive for electricity generation because of its noiseless, pollution-free, scale flexibility, and little maintenance [2]. It is global and can be harnessed without using rotational generators. PV generator is composed of a various number of solar cells connected like series and parallels [3]. Because of the PV power generation dependence on sun irradiation level, ambient temperature, and unpredictable shadows, a PV-based power system should be supplemented by other alternative energy sources to ensure a reliable power supply [4]. wind turbines generation system are emerging as a promising supplementary power sources due to their merits of cleanness, high efficiency, and high reliability.

There are sevaeral tube of generators that are used in wind turbines. The most popular one is doubly fed induction generator (DFIG). It has converters rated at about 25%–30% of the generator rating. It also offers several advantages including four-quadrant active and reactive power capabilities [5], variable speed operation through the rotor side converter (RSC) and grid side converter (GSC) [6, 7]. Such system results in lower converter costs and lower power losses compared to a system based on a fully fed synchronous generator with full-rated converter.

Because some of renewable energy sources can complement each other, multi-source alternative energy systems have great potential to provide higher quality and more reliable power to consumers than a system based on a single source [8]. Systems based on either wind or solar energy is unreliable due to seasonal and diurnal variations of these resources. A hybrid system is composed of two or more renewable energy resources with appropriate energy conversion technology connected together to feed power to local load or to the grid [9].

In fact, wind power and PV power are complementary to some point since tough winds are regularly to happen during the night-time and cloudy days whereas sunny days are often calm with weak winds [10]. Hence, a PV-Wind hybrid generation system can offer higher reliability to maintain continuous power output than any other

iJETRM
International Journal of Engineering Technology Research & Management

individual power generation systems [11, 12]. Therefore, this study is orientated towards grid-connected PV-Wind energy generation systems.
This paper is organized as follows: the proposed hybrid system configuration is presented in section II. Section III shows the modeling of DFIG. control scheme for rotor-side and grid-side converters is presented in section IV and section V respectively. System validation/verification is carried out through simulation results in section VI. Section VII gives the conclusions drawn from this research.

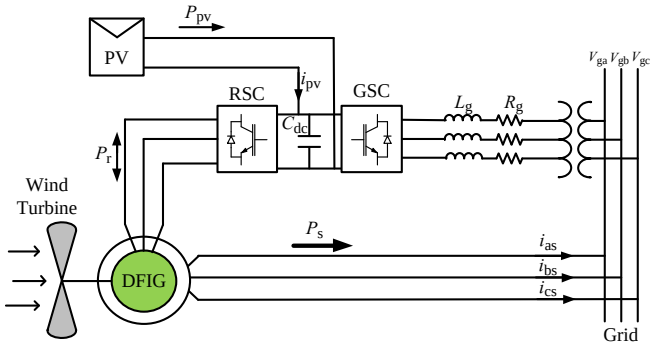

Fig. 1: The Proposed Solar PV-Wind Energy System Based DFIG.

THE PROPOSED HYBRID SYSTEM

The hybrid PV-wind energy generation system overcomes several drawbacks of the individual PV and wind energy sources. An inherent advantage of hybrid solar PV-wind energy system is the reduction in the overall variation in the power output. Fig. 1 shows the proposed scheme. The GSC and RSC associated with DFIG are used to inject PV generated power into the grid. A PV solar is connected to the dc-link between the RSC and the GSC. The RSC is connected to the terminals of DFIG for the maximum power tracking. The GSC is connected to the stator terminals of DFIG and the grid through a delta-star transformer. The transformer operates as a shunt active power filter for compensating harmonics.
The system advantages can be summarized as follows :

- Elimination of the dedicated inverter for the PV source and its associated control circuit are eliminated. This in turn reduces the overall cost of the system.
- Optimization of the power converters utilization.
- Facilitation of the possible interfacing for higher rating PV source compared to the dedicated inverter in the conventional interface.
- Reduction of the circulating power flow in the DFIG system during low speed operation and high solar radiation. This cuts down the losses of the overall system, and enhances the overall system efficiency.
- Realization of the Maximum extracted power from PV in conjunction with the dc bus voltage control.
- Controlling the pitch angle of the wind turbine to avoid overloading in case of high wind velocity, and also for maximum power extraction from the wind.
- Minimization of the grid-injected power Variation over a day.
- The proposed hybrid system has scope for integration of energy storage for enhancing power quality and reliability in terms of continuity and availability of the power supply. The overall power injection from this hybrid system to the grid is averaged by the intermittent but complementary sources of PV and wind
- A modified PV power control algorithm incorporated in the control scheme can tackle any of the environmental conditions in case of both high radiation and wind velocity level occurring simultaneously [13]. Thus, the proposed configuration and control scheme provide an elegant and economic integration of PV source and DFIG-based wind energy source.

MODELING OF DFIG

The dynamics of the DFIG is represented by a fourth-order state space model using the synchronously rotating reference frame (d-q frame) as given in (1)-(4) [14].

iJETRM
International Journal of Engineering Technology Research & Management

$$V_{qs} = R_s I_{qs} + w_s \Psi_{ds} + \frac{d}{dt}\Psi_{qs} \quad (1) \qquad V_{ds} = R_s I_{ds} - w_s \Psi_{qs} + \frac{d}{dt}\Psi_{ds} \quad (2)$$

$$V_{qr} = R_r I_{qr} + (w_s - w_r)\Psi_{dr} + \frac{d}{dt}\Psi_{qr} \quad (3) \qquad V_{dr} = R_r I_{dr} - (w_s - w_r)\Psi_{qr} + \frac{d}{dt}\Psi_{dr} \quad (4)$$

where V_{ds} , V_{qs}, V_{dr}, V_{qr} are the d-q axes stator and rotor voltages respectively. And I_{ds}, I_{qs}, I_{dr} , I_{qr} are the d-q axes stator and rotor currents respectively. Meanwhile, Ψ_{ds}, Ψ_{qs}, Ψ_{dr}, Ψ_{qr} are the d-q axes stator and rotor fluxes, respectively. w_s is the angular velocity of the synchronously rotating reference frame, w_r is rotor angular velocity, R_s and R_r are the stator and rotor resistances, respectively. The flux linkage equations are given by:

$$\Psi_{ds} = L_s I_{ds} + L_m I_{dr} \quad (5) \qquad \Psi_{qs} = L_s I_{qs} + L_m I_{qr} \quad (6)$$

$$\Psi_{dr} = L_m I_{ds} + L_r I_{dr} \quad (7) \qquad \Psi_{qr} = L_m I_{qs} + L_r I_{qr} \quad (8)$$

where L_s , L_r and L_m are the stator self, rotor self, and mutual inductance respectively. $L_s = L_{ls} + L_m$ and $L_r = L_{lr} + L_m$; L_{ls} being the stator leakage-inductance, and L_{lr} being the rotor leakage–inductance.

Solving (5), (8) in terms of current equations

$$I_{ds} = \frac{1}{\sigma_r L_s}\Psi_{ds} - \frac{L_m}{\sigma_r L_s L_r}\Psi_{dr} \quad (9) \qquad I_{qs} = \frac{1}{\sigma_r L_s}\Psi_{qs} - \frac{L_m}{\sigma_r L_s L_r}\Psi_{qr} \quad (10)$$

$$I_{dr} = -\frac{L_m}{\sigma_r L_s L_r}\Psi_{ds} + \frac{1}{\sigma_r L_r}\Psi_{dr} \quad (11) \qquad I_{qr} = -\frac{L_m}{\sigma_r L_s L_r}\Psi_{qs} + \frac{1}{\sigma_r L_r}\Psi_{qr} \quad (12)$$

where leakage coefficient $\sigma_r = \frac{L_s L_r - L_m^2}{L_s L_r}$ (13)

The expressions of the torque, active power and reactive power of the stator and the rotor using the new subscript expressions can be rewritten as follows:

$$T_{dev} = \frac{3}{2}\left(\frac{P}{2}\right)\left[\Psi_{ds} I_{qs} - \Psi_{qs} I_{ds}\right] \quad (14) \qquad P_s = \frac{3}{2}(V_{ds} I_{ds} + V_{qs} I_{qs}) \quad (15)$$

$$Q_s = \frac{3}{2}(V_{qs} I_{ds} - V_{ds} I_{qs}) \quad (16) \qquad P_r = \frac{3}{2}(V_{dr} i_{dr} + V_{qr} i_{qr}) \quad (17)$$

$$Q_r = \frac{3}{2}(V_{qr} i_{dr} - V_{dr} i_{qr}) \quad (18)$$

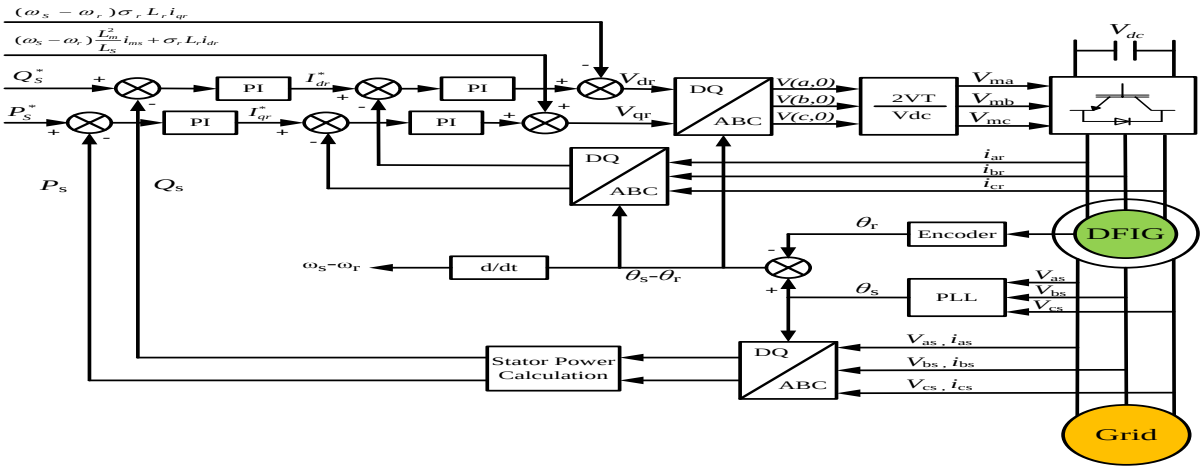

Fig. 2: Block Diagram For The Rotor-Side Converter Control.

iJETRM
International Journal of Engineering Technology Research & Management

CONTROL SCHEME FOR ROTOR SIDE CONVERTER

Figure 2 shows the overall vector control scheme of the RSC in which the independent control of the stator active power P_s and reactive power Q_s is achieved by means of rotor current regulation in a stator-flux-oriented synchronously rotating reference frame [15,16].

Also RSC control allows the wind turbine to control the DFIG rotor speed. This facilitates high flexibility which enables the turbine to capture maximum energy from wind and at the same time to provide reactive power support to the grid [16]. Under the stator flux control scheme, all the stator and rotor variables are needed to be converted to the synchronously rotating stator flux reference frame. In the stator-flux oriented reference frame, the d-axis is aligned with the stator flux linkage vectorΨ_s, namely, $\Psi_{ds} = \Psi_s$ and $\Psi_{qs} = 0$. This gives the following relationships [13, 17]:

$$|\Psi_s| = \Psi_{ds} = L_m i_{ms} \quad (19) \qquad i_{ds} = \frac{L_m i_{ms} - L_m i_{dr}}{L_s} \quad (20) \qquad i_{qs} = -\frac{L_m}{L_s} i_{qr} \quad (21)$$

where,i_{ms} is the magnetizing current of DFIG.

$$\Psi_{dr} = \frac{L_m^2}{L_s} i_{ms} + \sigma_r L_r \quad (22) \qquad \Psi_{qr} = \sigma_r L_r i_{qr} \quad (23)$$

$$v_{dr} = R_r i_{dr} + \sigma_r L_r \frac{di_{dr}}{dt} - (w_s - w_r)\sigma_r L_r i_{qr} \quad (24)$$

$$v_{qr} = R_r i_{qr} - (w_s - w_r)\left(\frac{L_m^2}{L_s} i_{ms} + \sigma_r L_r i_{dr}\right) + \sigma_r L_r \frac{di_{qr}}{dt} \quad (25)$$

The q-axis of the rotating reference frame is aligned to the stator voltage i.e. $v_{ds} = 0$ and $v_{qs} = |v_s|$.The develop torque, stator active and reactive power can be expressed as:

$$T_{dev} = \frac{3}{2}\frac{p}{2}\Psi_{ds} i_{qs} = -\frac{3}{2}\frac{p}{2}\frac{L_m^2}{L_s} i_{ms} i_{qr} \quad (26) \qquad P_s = \frac{3}{2} v_{qs} i_{qs} = -\frac{3}{2}|v_s|\frac{L_m}{L_s} i_{qr} \quad (27)$$

$$Q_s = \frac{3}{2} v_{qs} i_{ds} = \frac{3}{2}|v_s|\frac{L_m}{L_s}(i_{ms} - i_{dr}) \quad (28)$$

The control signals for the RSC can be developed and written as follows:

$$v_d = \Delta v_{dr} - (w_s - w_r)\sigma_r L_r i_{qr} \quad (29) \qquad v_q = \Delta v_{qr} + (w_s - w_r)\left(\frac{L_m^2}{L_s} i_{ms} + \sigma_r L_r i_{dr}\right) \quad (30)$$

$$\Delta v_{dr} = k_p(i_{dr}^* - i_{dr}) + k_i \int (i_{dr}^* - i_{dr}) d \quad (31)$$

$$\Delta v_{qr} = k_p\left(i_{qr}^* - i_{qr}\right) + k_i \int (i_{qr}^* - i_{qr}) d \quad (32)$$

CONTROL SCHEME FOR GRID-SIDE CONVERTER AND PV POWER

In DFIG wind turbine, the GSC controls the dc-link voltage and contributes to the reactive power or grid voltage support control of the overall DFIG system as well [18]. In the d-q reference frame the GSC current model, is represented by:

$$L_g \frac{di_{gd}}{dt} = -R_g i_{gd} + L_g w_s i_{gq} - \frac{V_{DC}}{2} m_{gd} + v_{gd} \quad (33)$$

$$L_g \frac{di_{gq}}{dt} = -R_g i_{gq} - L_g w_s i_{gd} - \frac{V_{DC}}{2} m_{gq} + v_{gq} \quad (34)$$

where m_{gd} and m_{gq} are the modulation indices.

iJETRM
International Journal of Engineering Technology Research & Management

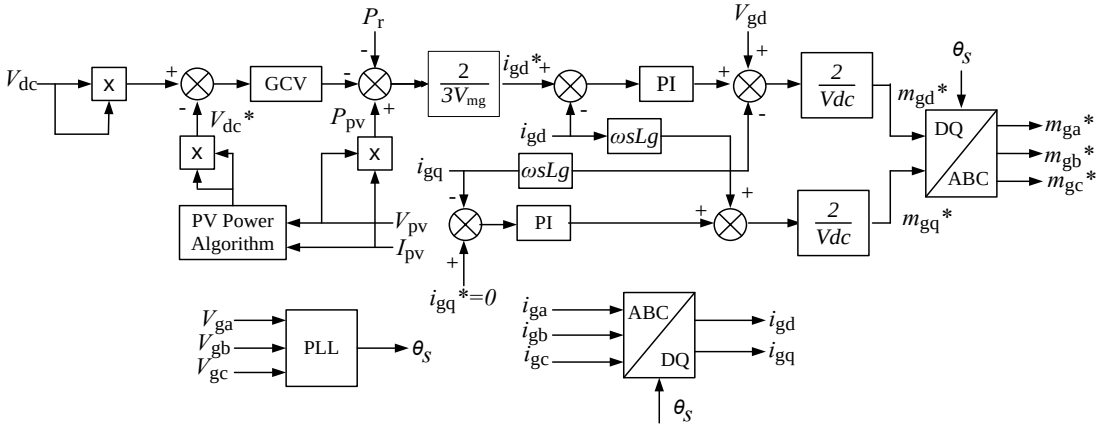

Fig. 3: Proposed Control Strategy For The Grid-Side Converter.

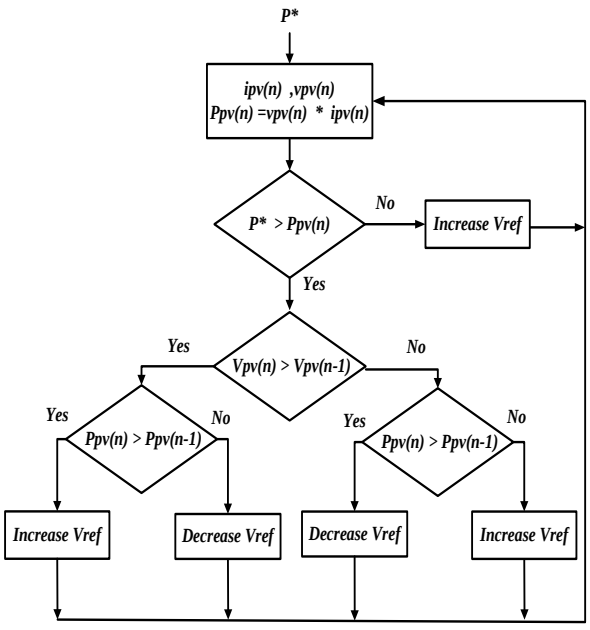

Fig.4: PV Power Control Algorithm for the Proposed Hybrid System.

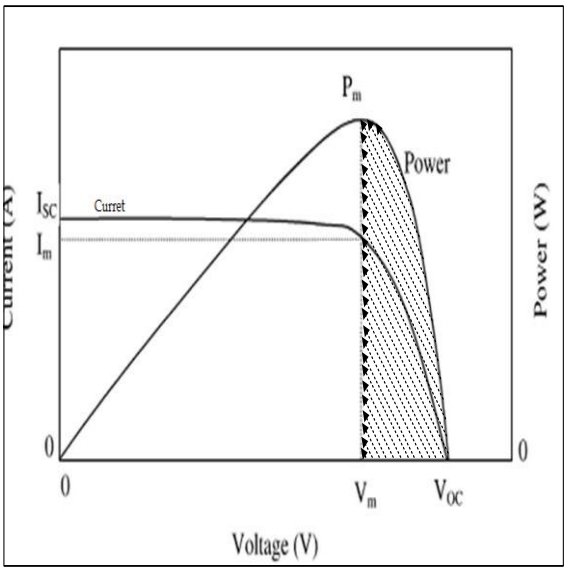

Fig. 5: The Controlled Operational Region for the PV System

In this case, d-axis of reference frame is aligned with the voltage vector, i.e, $v_{qs} = 0$. New variables Y_{gd} and Y_{gq}can be introduced in (33) and (34) to obtain the transfer function, G_{ig} to enable the design of the inner current loops as follows:

$$G_{ig} = \frac{I_{gd}(s)}{Y_{gd}(s)} = \frac{I_{gq}(s)}{Y_{gq}(s)} = \frac{1}{L_g s + R_g} \quad (35)$$

From (33) and (34) the modulation indices m_{gd} and m_{gq} can be expressed as follows to incorporate decoupling and feed forward compensation:

$$m_{gd} = \frac{-2}{V_{DC}}(y_{gd} - L_g w_s i_{gq} - v_{gd}) \quad (36)$$

$$m_{gq} = \frac{-2}{V_{DC}}(y_{gq} + L_g w_s i_{gd}) \quad (37)$$

iJETRM
International Journal of Engineering Technology Research & Management

G_{cig} is used to design the PI compensator for the inner current control loop of grid side converter. Thus, elements of G_{cig} are: $K_{Pig} = \frac{L_g}{T_{cig}}$; $K_{Iig} = \frac{R_g}{T_{cig}}$ (38)

Where K_{Pig} and K_{Iig} are the PI controller's proportional and integral parameters respectively. With the previous compensator parameters, the closed-loop transfer function of the current control loop GCL can be reduced to first order with unity gain as follows: $G_{CL}(s) = \frac{1}{T_{cig}S+1}$ (39)

Plant model for the PV terminal (dc link) voltage control can be determined from the power balance condition across the dc and ac ports of GSC as follows

$$P_{pv} = \frac{d}{dt}\frac{1}{2}C_{DC}{v_{DC}}^2 + P_r + \frac{3}{2}v_{gd}i_{gd} \quad (40)$$

Assuming the inner current control loop of GSC to be considerably faster (T_{cig} is small), the reference, i_{gd}^* is used as the controlling parameter for dc-bus voltage regulation. V_{DC}^2 is state as well as an output variable while i_{gd}^* is the control variable and input to the inner current control loop. Using a new variable $\mathrm{p_h}$, the transfer function $\mathrm{G_V}$ can be written as follows:

$$G_V(S) = \frac{V_{DC}^2(S)}{P_h(S)} = \frac{2}{C_{DC}S} \quad (41)$$

Where ${i_{dg}}^*$ is related to $\mathrm{p_h}$ as follows:

$$i_{gd}^* = \frac{2}{3V_{gd}}(-p_h + P_{PV} - P_r) \quad (42)$$

Rotor power P_r and PV-power P_{pv} from measurement may be provided for feed-forward compensation to improve dynamic response against disturbances. The loss component of the converter and that of dc-link cannot be measured. Therefore, the integral term is added with a lead compensator to achieve zero steady-state error and sufficient phase margin. A phase boost ($\emptyset_{\mathrm{Boost}}$) at the required cut-off frequency (WCV) of the gain plot can be designed such that WCV ≈0.1 to 0.3×1/Tcig. Thus,$\mathrm{G_{CV}}$ has the following form: $G_{CV}(s) = \frac{h}{s}\frac{s+r/\alpha}{s+r}$ (43)

where $r = WCV\sqrt{\alpha}$, $\alpha = \frac{1+sin\emptyset_{Boost}}{1-sin\emptyset_{Boost}}$ and h is adjusted such that the gain plot cuts the frequency axis at WCV. The GSC control strategy is shown in Fig. 3. The inner loop for grid-side current control and the outer loop for dc-link (PV terminal) voltage control.

V_{DC} was assumed to be a constant for the design of inner current control. In the proposed scheme, PV power is controlled by regulating V_{DC} and ensuring that the operation does not shift to the over modulation range. The PV power control algorithm for the proposed hybrid PV-wind system is illustrated in Fig. 4. Where, the reference power $(\mathrm{P}^* = P_{GSC} - P_r)$. The MPPT can be achieved for optimum power and also precise power control depending upon the operating mode, environmental conditions, and GSC loading. The shaded part in Fig. 5 shows the operation region for the PV system. This means when the wind speed increases over the rated value in the same time the irradiance is at its maximum value, the PV voltage is increased in order to shift the PV operating point shifts from MPP to avoid overloading of the grid side converter.

The GSC is an group of electronic switchs (IGBTs, SCR,….) that have a limtted overload capability. Thus, to improve the system response in the worest operational region (high wind speeds & high irradiance), the non-linear characterestics of the PV panels is used to train an artificial nerural network (ANN) to control the DC-link voltage directly without any iterative solution.
The DC-link voltage can be predicted accurately from a given PV power using artificial intelligent. one input, one hidden layer, and one output layer feed-forward neural network. For this problem, the network uses the Levenberg-Marquardt algorithm for training with thirteen neurons for the hidden layer.

iJETRM
International Journal of Engineering Technology Research & Management

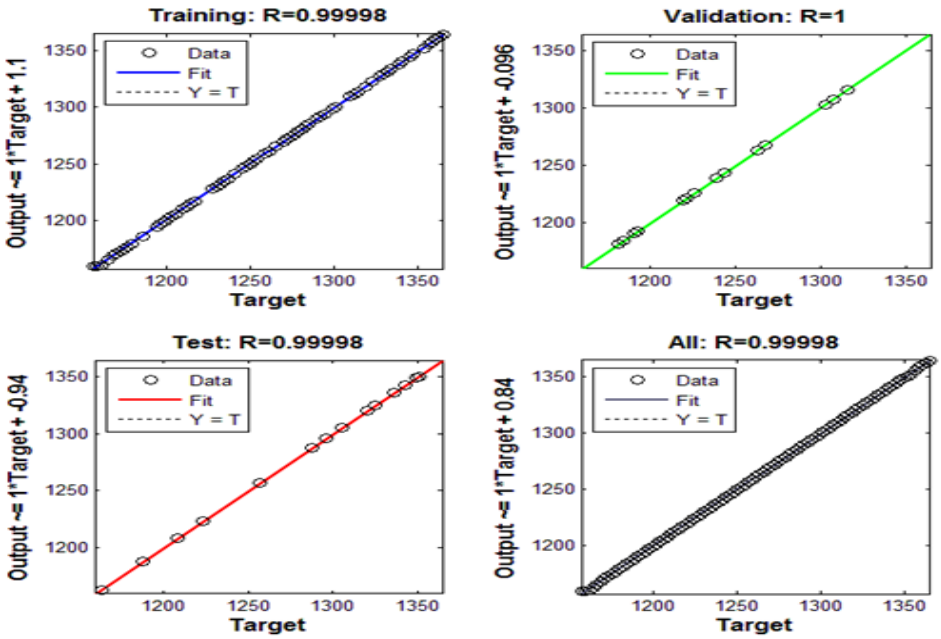

FIG. 6. REGRESSION OF THE TRAINED NEURAL NETWORK

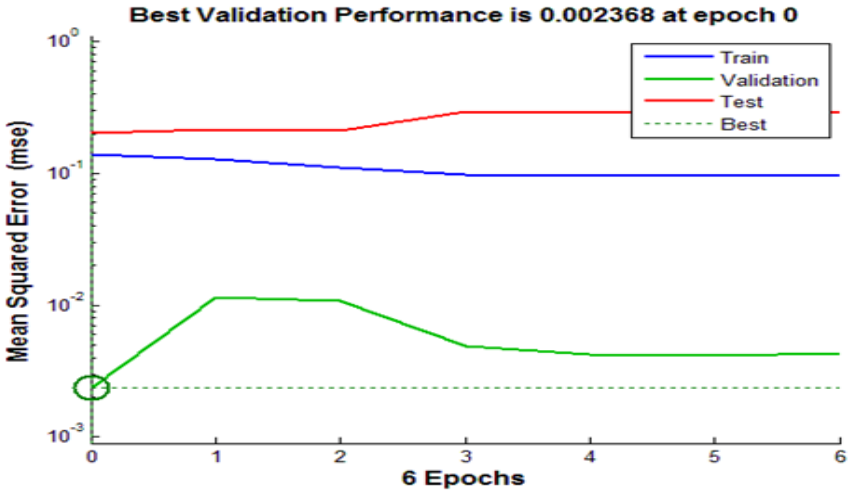

FIG. 7. PERFORMANCE OF TRAINING

The network can solve more complicated problems with more neurons in the hidden layer, but requires more computations [19]. The number of hidden layer neurons is decided after covering some simulation experiments with different number of neurons. Fig. 6 shows linear regression performance between network output and corresponding targets, it shows that the output tracks the targets very well for training, testing and validation and the R-value is over 0.9999 for the total response. Fig. 7 shows the training performance, it shows that final means square error is small and the network can work in efficient way. Result of training performance and regression performance dedicate that response of the network is satisfactory and network is ready to estimate the current for any input vector so network model and Simulink model of the neural network is generated.

The proposed control scheme for the GSC differs from the conventional control schemes in the following points:

iJETRM
International Journal of Engineering Technology Research & Management

- A modified PV power control algorithm has been inserted in the control scheme presented for GSC in the proposed system, and not just a conventional MPPT control.
- An additional control loop has been inserted to tackle the "worst case" environmental impact (high solar radiation and high wind speed existing at the same time) by automatically adjusting GSC loading.
- The PV and the wind systems operate at MPP during most of the time. However, during a harsh sunny day and heavy wind conditions occurring simultaneously, the PV operating point shifts from MPP in order to avoid overloading of GSC [13].

The parameters of the hybrid system and the final form of controllers determined from the previous procedure are presented in appendix.

SIMULATION RESULTS AND DISCUSSION

In this section, dynamic performance of the complete control scheme for various stages of the proposed hybrid PV/DFIG system is evaluated. The complete system is modeled in MATLAB/Simulink environment for verification/validation purpose. The complete system parameters are listed in the appendix.
To evaluate the important aspects of the proposed system, wind velocity and hence turbine speed are varied in the regions of sub synchronous and super synchronous speed so as to cover most frequently occurring events (including worst case) as shown in Fig.8 (a) by keeping turbine-machine combined inertia very low and directly controlling the speed parameter of the inbuilt MATLAB model. The solar irradiance is kept constant at (1000 w/m2) as shown in the same figure. While the wind speed varies from 6 m/s to 14m/s (over the rated) and also from 14m/s to 8m/s. When the wind speed is under the rated value of 12m/s (sub synchronous operation)
From t=(0-1.2 sec), and from t=(1.8-3sec) the dc link voltage is controlled according to the reference voltage which is equal to the voltage at max power of solar PV (VMP). When the wind speed is over the rated (super synchronous operation), the PV algorithm controls the flow of PV power so as to prevent the overloading of grid side converter by controlling dc-link voltage and hence PV terminal voltage. This may be seen during the interval t=(1.2-1.8 sec) as shown in Fig. 8(b)

Figure 8(c) shows the active and reactive powers of the DFIG stator windings. It can be seen that when the wind speed increase above 12m/s (super synchronous), the active power varies strongly with the wind speed to its rated value according to pitch control. The reactive power is controlled to achieve unity power factor. It has noticed fluctuations at the transient periods and zero in the remaining.
The rotor active power (P_r) under constant irradiance is shown in Fig. 8(d). Due to low wind speed (sub synchronous mode), the rotor power is positive and it is absorbed from the grid via the GSC and delivered to the rotor via the RSC. On the other hand, when the wind speed is becomes over the rated speed (super-synchronous), the rotor gives its active power to the grid during the intervals t=(1.2-1.8 sec).
Figure 8(e) show the power extracted from the PV system. It always equal to the maximum value but during high wind velocity and high radiation occurring simultaneously
From (1.2-1.8 sec) the PV power shifts from the maximum on the stiff slope of PV power to avoid overloading of the grid side converter.
The active and reactive power of the GSC is shown in Fig 8(f). In sub synchronous mode (0-1.2 sec and 1.8-3 sec), GSC absorbs active power from the grid to fed the rotor. On the other hand during super synchronous mode, (1.2-1.8 sec), the rotor give its power to the grid through GSC. The reactive power is controlled to achieve the unity power factor so it still equal to zero .The total active power injected to the grid is shown in Fig. 8(g). Figure 8(h) shows the stator current profile. As the grid voltages are constant, the stator current profile reflects the stator power variation. In super synchronous mode (1.2-1.8 sec), the pitch controls the DFIG power (current) to its rated value. The rotor current profile illustrated in Fig.8 (i). The d-q component of the rotor current is depicted in Fig.8 (j). Fig. 8 (k) shows the voltage at the PV terminal and it illustrates that when the wind speed increase over the rated value from(1.2-1.8 sec) in the same time the irradiance is constant at its maximum value (1000 w/m2) the PV voltage is increased because the PV operating point shifts from MPP so as to avoid overloading of the grid side converter while its current is illustrated by Fig.8 (l).

iJETRM
International Journal of Engineering Technology Research & Management

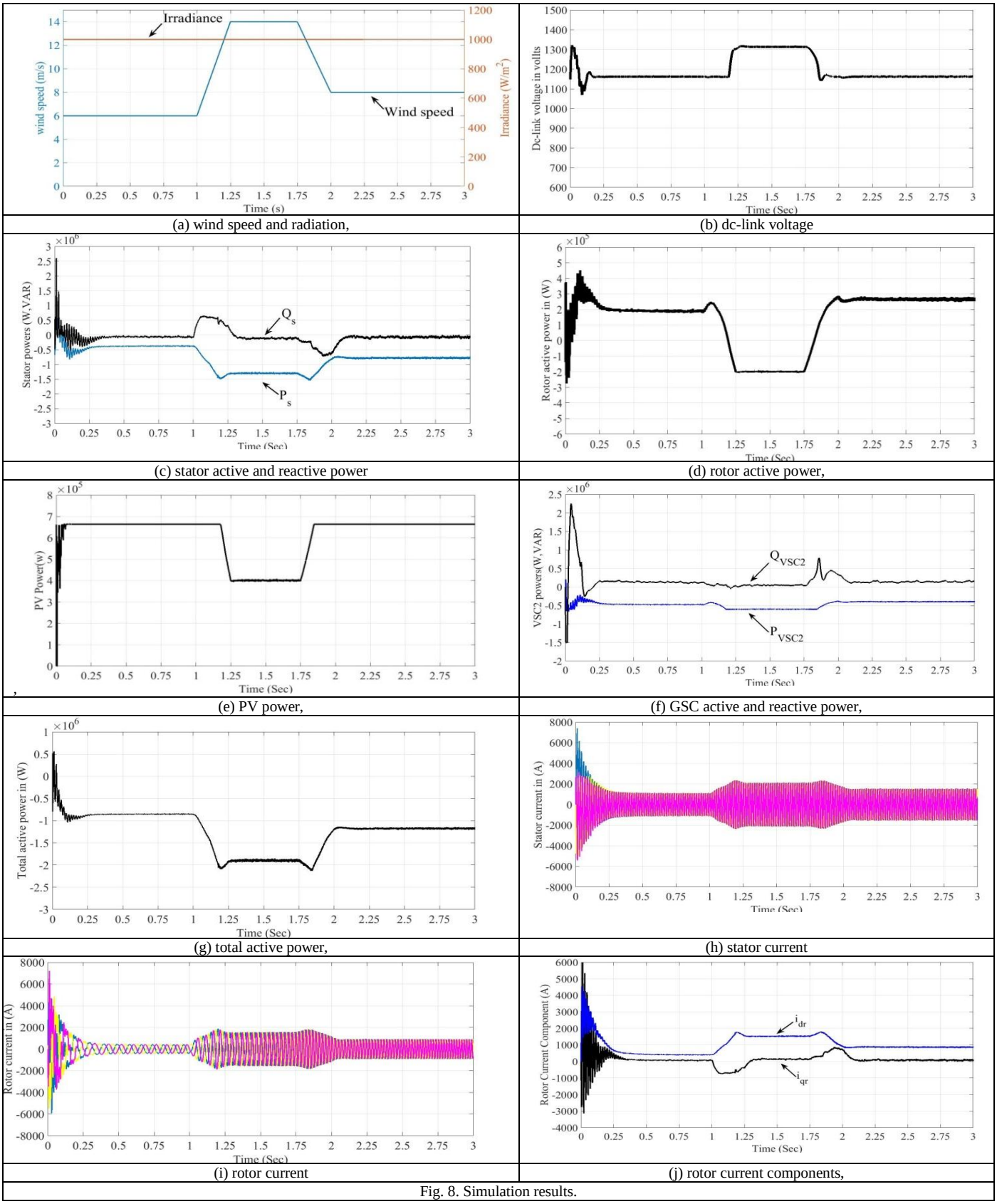

(a) wind speed and radiation,
(b) dc-link voltage
(c) stator active and reactive power
(d) rotor active power,
(e) PV power,
(f) GSC active and reactive power,
(g) total active power,
(h) stator current
(i) rotor current
(j) rotor current components,

Fig. 8. Simulation results.

iJETRM
International Journal of Engineering Technology Research & Management

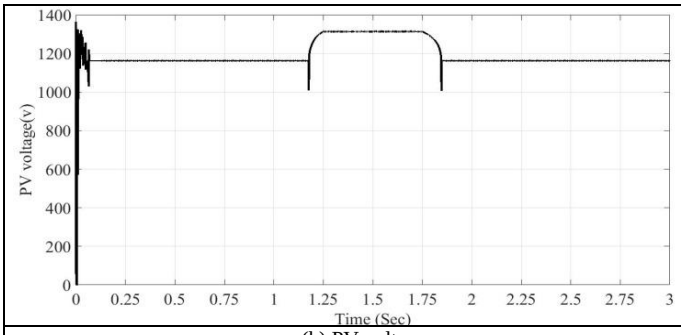

(k) PV voltage,

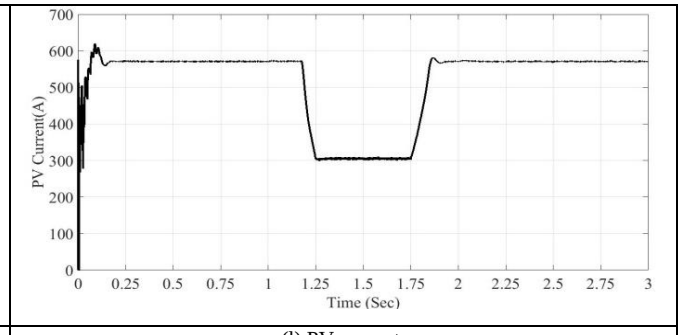

(l) PV current.

Continued Fig. 8. Simulation results.

CONCLUSION

The hybrid system based DFIG variable speed wind and PV energy conversion system has been successfully developed to overcome several drawbacks of the individual PV and wind energy sources. This paper shows how the integrated GSC and RSC control is designed to implement the maximum power extraction, the dc-link voltage control, active and reactive power, and grid voltage support control functions. The hybrid system with MPPT has been implemented and simulated using MATLAB/ Simulink environment. The system has been tested for different wind speed and PV irradiations conditions. The simulation results have been analyzed, it is shown that the generation system will supply constant voltages with varying wind speed and irradiation. The PV and the wind systems operate at MPP during most of the time. Also results illustrate that the rotor active power varies under variable wind speed. In sub synchronous mode of operation, the rotor absorbed the active power from the grid or it absorbs a portion from the PV generated power. That in turn lowers the KVA rating of the GSC and also its cost. In super synchronous mode of operation, the rotor gives its power to the grid. This mode of operation happens at lower levels of solar irradiance. This in turn insures the overloading of GSC is mostly unexpected. At the worst cases of operation during a harsh sunny day and heavy wind conditions occurring simultaneously, the overloading of GSC can be controlled by reducing the PV generated power. The PV operating point shifts from MPP so as to avoid overloading of GSC. It's clear that the proposed system optimally making the best possible utilization of its converters and uses the daily available energy from solar and wind sources.

REFERENCES

[1] H. Xu, J. Hu and Y. He, "Operation of Wind-Turbine-Driven DFIG Systems under Distorted Grid Voltage Conditions: Analysis and Experimental Validations," IEEE Transactions on Power Electronics, Vol. 27, NO. 5, pp.2354–2366, May 2012.

[2] Krismadinata, N. Abd. Rahim, H. W. Ping, and J. Selvaraj, "Photovoltaic module modeling using Simulink/matlab," The 3rd International Conference on Sustainable Future for Human Security SUSTAIN 2012, pp.537–546, 2013.

[3] M. G. Villalva , J. R. Gazoli, and E. R. Filho, "Comprehensive Approach to Modeling and Simulation of Photovoltaic Arrays," IEEE Transactions on Power Electronics, Vol. 24, No. 5, pp. 1198– 1208, May 2009.

[4] F. Nejabatkhah ,S. Danyali,S.H. Hosseini,M. Sabahi ,and S.M. Niapour, "Modeling and Control of a New Three-Input DC–DC Boost Converter for Hybrid PV/FC/Battery Power System," IEEE Transactions on Power Electronics, Vol. 27, No. 5, pp.2309–2324, May 2012.

[5] J. Yao, H. Li, Y. Liao, and Z. Chen, "An Improved Control Strategy of Limiting the DC-Link Voltage Fluctuation for a Doubly Fed Induction Wind Generator," IEEE Transactions on Power Electronics, Vol. 23, No. 3, pp. 1205– 1213, May 2008.

[6] L. Xu, and P. Cartwright, "Direct Active and Reactive Power Control of DFIG for Wind Energy Generation," IEEE Transactions On Energy Conversion, Vol. 21, No. 3, pp. 750– 758, September 2006.

[7] H. Nian, and Y. Song, "Direct Power Control of Doubly Fed Induction Generator under Distorted Grid Voltage," IEEE Transactions on Power Electronics, Vol. 29, No. 2, pp. 1198– 1208, February 2014.

iJETRM
International Journal of Engineering Technology Research & Management

[8] P.K. Olulope, K.A. Folly, and G.K. Venayagamoorthy, "Modeling And Simulation of Hybrid Distributed Generation And Its Impact on Transient Stability of Power System," IEEE International Conference on Industrial Technology (ICIT), pp.1757–1762, Feb 2013.
[9] P. Gupta, and S. K. Tripathi, "Analysis of Grid-Tied Hybrid Wind PV Generation System," IEEE International Conference on Innovative Applications of Computational Intelligence on Power, Energy and Controls with their Impact on Humanity (CIPECH14), pp. 447–451, November 2014.
[10] Ashraf Abdel Hafeez Ahmed Mahmoud, "Power Conditioning Unit forSmallScale Hybrid PV-Wind Generation System," PhD thesis, Durham University, 2010, pp.189.
[11] T. Boutabba, S. Drid, and M.E.H. Benbouzid, "A Hybrid Power Generations System (Wind Turbine/Photovoltaic) to driving a DFIG fed by a three inverter," IEEE 15th International Conference on Sciences and Techniques of Automatic Control and Computer Engineering (STA), pp. 873–880, Dec. 2014.
[12] S. A. Daniel and N. A.Gounden, "A Novel Hybrid Isolated Generating System Based on PV Fed Inverter-Assisted Wind-Driven Induction Generators," IEEE Transactions on Energy Conversion, Vol. 19, NO. 2, pp.416–421, June 2004.
[13] R.G. Wandhare, and V. Agarwal, "Novel Integration of a PV-Wind Energy System with Enhanced Efficiency," IEEE Transactions on Power Electronics, Vol. 30, No. 7, pp.3639–3649, July 2015.
[14] L. Xu, D. Zhi, and B. W. Williams, "Predictive Current Control of Doubly Fed Induction Generators," IEEE Transactions on Industrial Electronics, Vol. 56, No. 10, pp. 4143– 4153, October 2009.
[15] L. Qu, and W. Qiao, "Constant Power Control of DFIG Wind Turbines With Supercapacitor Energy Storage," IEEE Transactions on Industry Applications, Vol. 47, No. 1, pp. 359-367, February 2011.
[16] Ab. Hamadi, S. Rahmani, K. Addoweesh and K. Al-Haddad, "A Modeling And Control Of DFIG Wind And PV Solar Energy Source Generation Feeding Four Wire Isolated Load," 39th Annual Conference of the IEEE Industrial Electronics Society, IECON, pp. 447–451, November 2013.
[17] W. Qiao, "Dynamic Modeling and Control of Doubly Fed Induction Generators Driven by Wind Turbines," IEEE Power Systems Conference and Exposition, pp.1–8, March 2009.
[18] S. Li, T.A. Haskew, K. A. Williams and R. P. Swatloski, "Control of DFIG Wind Turbine with Direct-Current Vector Control Configuration," IEEE Transactions on Sustainable Energy, Vol. 3, NO. 1, pp. 1–11, January 2012.
[19] B. M. Alluhaidah, S. H. Shehadeh, and M. E. El-Hawary, "Most Influential Variables for Solar Radiation Forecasting Using Artificial Neural Networks," 2014 IEEE Electr. Power Energy Conf., pp. 71–75, 2014.

APPENDIX

Parameter		*Value*
PV capacity	(MW)	0.6
Nominal power	(MW)	1.5
Nominal L-L voltage	(V)	575
Nominal frequency	(HZ)	60
Number of pole pairs		3
Stator leakage inductance	(pu)	0.18
Stator resistance	(pu)	0.023
Rotor leakage inductance	(pu)	0.16
Rotor resistance	(pu)	0.016
Magnetising inductance	(pu)	2.9
Lumped friction constant	(pu)	0.01
Lumped inertia constant	($Nm.s^2$)	0.685
DC-link voltage	(V)	1150
DC-link capacitor	(µF)	100000
V_{mp}at 1000 W/m	(V)	1160
GSC current controller		$G_{cig}(s) = (0.88s + 65)/s$